

Paper published in:

T.M.H. Le, M. Sánchez, D. Gallipoli and S. Wheeler (2019).

Probabilistic Study of Rainfall-Triggered Instabilities in Randomly Heterogeneous

Unsaturated Finite Slopes.

Transport in Porous Media, 126(1): 199–222

<https://doi.org/10.1007/s11242-018-1140-0>

**Probabilistic study of rainfall-triggered instabilities in randomly heterogeneous
unsaturated finite slopes**

AUTHORS:

Thi Minh Hue Le¹, Marcelo Sanchez², Domenico Gallipoli³, Simon Wheeler⁴

AFFILIATIONS:

¹ Norwegian Geotechnical Institute. Sognveien 72, Oslo, Norway; Tel: +47 (0) 9300 1834; Email: thi.le@ngi.no

² Zachry Department of Civil Engineering, Texas A&M University, 3136 TAMU, College Station, TX 77843-3136, United States; Tel. (+1) -979- 862 6604; Fax: (+1) -979- 862 7696; Email: msanchez@civil.tamu.edu

³ Laboratoire SIAME, Fédération IPRA, Université de Pau et des Pays de l'Adour, Fédération IPRA, Allée du Parc Montaury, Anglet, 64600, France; Tel : +33 (0)559574280; Email: domenico.gallipoli@univ-pau.fr

⁴ Infrastructure & Environment Research Division, School of Engineering, University of Glasgow, G12 8LT, Glasgow, United Kingdom; Tel: +44 (0)141 330 5201; Fax: +44 (0)141 330 4557; Email: Simon.Wheeler@glasgow.ac.uk

Abstract

Water infiltration destabilises unsaturated soil slopes by reducing matric suction, which produces a decrease of material cohesion. If the porosity of the soil is spatially heterogeneous, a degree of uncertainty is added to the problem as water tends to follow preferential paths and produces an irregular spatial distribution of suction. This study employs the finite element method together with Monte Carlo simulations to quantify the effect of random porosity on the uncertainty of both the factor of safety and failure size of an unsaturated finite slope during and after a rainfall event. The random porosity is modelled using a univariate random field. Results show that, under partially saturated conditions, the random heterogeneity leads to a complex statistical variation of both factor of safety and failure size during the rainfall event. At any given time, the uncertainty about failure size is directly linked to the uncertainty about the position of the wetting front generated by infiltration. Interestingly, the statistical mean of the failed area is smallest when the mean of the factor of safety is lowest. In other words, the slope becomes more likely to fail but the size of the failure mass tends to be limited.

The study also investigates the sensitivity of failure uncertainty to external hydraulic parameters (i.e. initial water table depth, rainfall intensity) and internal soil parameters (i.e. permeability and water retention characteristics). In general, the sensitivity increases when the effect of these parameters on the spatial variation of suction is stronger.

1 Introduction

Catastrophic failures of soil slopes caused by rainfall infiltration are relatively common but their triggering mechanisms are still poorly understood. This is particularly true in unsaturated slopes where the spatial variability of suction and degree of saturation induces an uneven distribution of permeability inside the soil mass. This also means that, unlike in saturated soils, the permeability of unsaturated soils does not remain constant during the rainfall. The high non-linearity of the constitutive equations linking the soil suction (or saturation) to permeability and the coupling between soil porosity and degree of saturation make the numerical solution of these problems very challenging.

Further complexities are introduced by the heterogeneity of porosity, which influences the infiltration pattern and hence the stability of the slope. In a heterogeneous slope, water will preferably infiltrate through paths connecting high permeability areas, which in turn produces a spatially irregular distribution of suction and saturation inside the soil mass (Le et al. 2012). Soil elements experiencing an earlier loss of suction will also undergo an earlier reduction of strength compared to other elements where suction changes are slower. At any given time, the likely slip surface will therefore tend to pass through these weaker elements, which may result in a lower safety factor compared to a homogenous slope.

A relatively large number of probabilistic studies have investigated the effect of material uncertainties on the safety of dry or saturated slopes. Many of them have employed the finite element method (FEM), which is particularly suited to the description of spatial heterogeneity, to analyse the effect of strength variability on slope safety (Hicks 2005; Griffiths and Fenton 2004). Other studies have instead employed the limit equilibrium method (LEM) because of its simplicity (Pathak et al. 2007; El-Ramly et al. 2005). Stochastic studies of slope instabilities in randomly heterogeneous slopes have relied on Monte Carlo simulations to handle complicated geometries and variability patterns without requiring over-simplified assumptions. Results from these simulations, and from

practical observations, have repeatedly indicated that material heterogeneity affects strongly the stability of soil slopes (Alonso 1976; Babu and Mukesh 2004; El-Ramly et al. 2005; Griffiths and Fenton 2004; Griffiths and Marquez 2007; Hicks and Onisiphorou 2005; Hicks and Samy 2002; Hicks and Spencer 2010; Mostyn and Li 1993; Mostyn and Soo 1992; Sejnoha et al. 2007; Cho 2009; Fenton and Griffiths 2005; Griffiths et al. 2015). The majority of stochastic studies adopted the Monte Carlo approach because of its conceptual simplicity and its capability to handle complicated geometry and variability patterns without requiring over-simplified assumptions. A number of works based on Monte Carlo simulation have yielded a full description of the shearing processes and the probability of failure or the reliability of fully saturated heterogeneous slopes (Griffiths and Fenton 2004; Griffiths and Marquez 2007; Hicks and Onisiphorou 2005; Hicks and Samy 2002).

There have been a number of studies investigating the influence of rainfall intensity, water table and permeability on the stability of saturated slope (e.g., Tsaparas et al. (2002)). The main findings from these works cannot be directly applied to unsaturated slopes, because the flow characteristics in unsaturated soils are different from the ones observed under saturated conditions. Past studies on unsaturated slope stability are mostly limited to homogeneous soil properties and were conducted using different approaches, including analytical solution, the LEM and the FEM. Griffiths and Lu (2005) and Lu and Godt (2008) suggested a formula based on suction stress that takes into account both, the soil characteristics and the infiltration rate. The suction stress was then used to analytically predict the stability of an infinite unsaturated slope in a steady seepage condition. Ng and Shi (1998) conducted a LEM parametric study to investigate the effect of various hydraulic parameters, amongst others: permeability, rainfall intensity, infiltration duration and boundary conditions. It was observed that soil permeability and rainfall characteristics (i.e. intensity and duration) could have significant influences on the stability of unsaturated slopes. Importantly, the factor of safety can reduce considerably with the relative differences in magnitude between the soil permeability and the rainfall intensity and it might also depend on permeability anisotropy.

Few studies have also attempted to incorporate material uncertainties into a stochastic analysis of partly saturated slopes. Among these studies, some are limited to the analysis of infinite slopes with one-dimensional random variations of permeability (Santoso et al. 2011; Dou et al. 2014; Cho and Lee 2001; Cho 2014; Xia et al. 2017). For example, Dou et al. (2014) employed a Green-Ampt infiltration model to obtain a closed form of the limit state function of an infinite slope. The Monte Carlo simulation method was then used to study the influence of saturated permeability on slope failure during rainfall. Xia et al. (2017) adopted a stochastic method to predict the risk of failure of an infinite unsaturated slope subjected to rainfall. They proposed an analytic solution and compared it against a Monte Carlo simulation.

Sensitivity analyses looking at the effect of different factors (e.g. slope angle, water table position, soil air entry value, dry density and specific density) on slope failure were also conducted. Zhang et al. (2005) developed a coupled hydro-mechanical finite element model to study the effect of the variability of different constitutive parameters. Zhang et al. (2014) also extended this model to the analysis of rainfall intensity-duration and suggested a framework for predicting time-dependent failure probability. Arnold and Hicks (2010) studied the effect of the random variability of friction angle, cohesion, porosity, saturated permeability and air entry suction on the stability of a finite unsaturated slope. Phoon et al. (2010) proposed a probabilistic model of normalised soil water retention curve (SWRC), whose shape and air entry value were modelled by a correlated lognormal vector. The study did not however take into account the variability of saturated permeability. Santoso et al. (2011) further developed the SWRC model proposed in Phoon et al. (2010) by incorporating the saturated water content as an additional random variable. The Kozeny-Carman equation was adopted to link the random saturated water content to the saturated permeability. This approach implies that the shape of the SWRC and the saturated permeability are independent from one another, while in the present study they are coupled through the porosity as described later.

A limited number of authors have also investigated the depth of the failure zone. Alonso and Lloret (1983) showed that the slope angle marking the transition from shallow to

deep failure increases with soil dryness. Hicks et al. (2008) presented a three-dimensional stochastic study of the size of the sliding area in saturated slopes. Santoso et al. (2011) demonstrated instead that shallow failure mechanisms in randomly heterogeneous infinite unsaturated slopes cannot be predicted using a homogeneous slope model. Finally, Le et al. (2015) evaluated the effect of the standard deviation and correlation length of random porosity on the size of the sliding area in an unsaturated slope.

Following upon earlier studies, the present work investigates the effect of external and internal factors on the uncertainty of the factor of safety and failure size in unsaturated slopes with randomly heterogeneous porosity. These factors include external environmental conditions (i.e. water table depth and rainfall intensity) and internal soil parameters (i.e. saturated permeability and water retention characteristics). Importantly, unlike random saturated soils, preferential water pathways do not necessarily coincide with the most porous regions (Le et al. 2015). These regions might in fact exhibit smaller values of permeability because of lower saturation levels. A fully coupled hydro-mechanical FE code is adapted to perform the numerical simulations involving a finite slope. The Monte Carlo method is adopted to conduct the probabilistic study.

2 Method

2.1 Model geometry

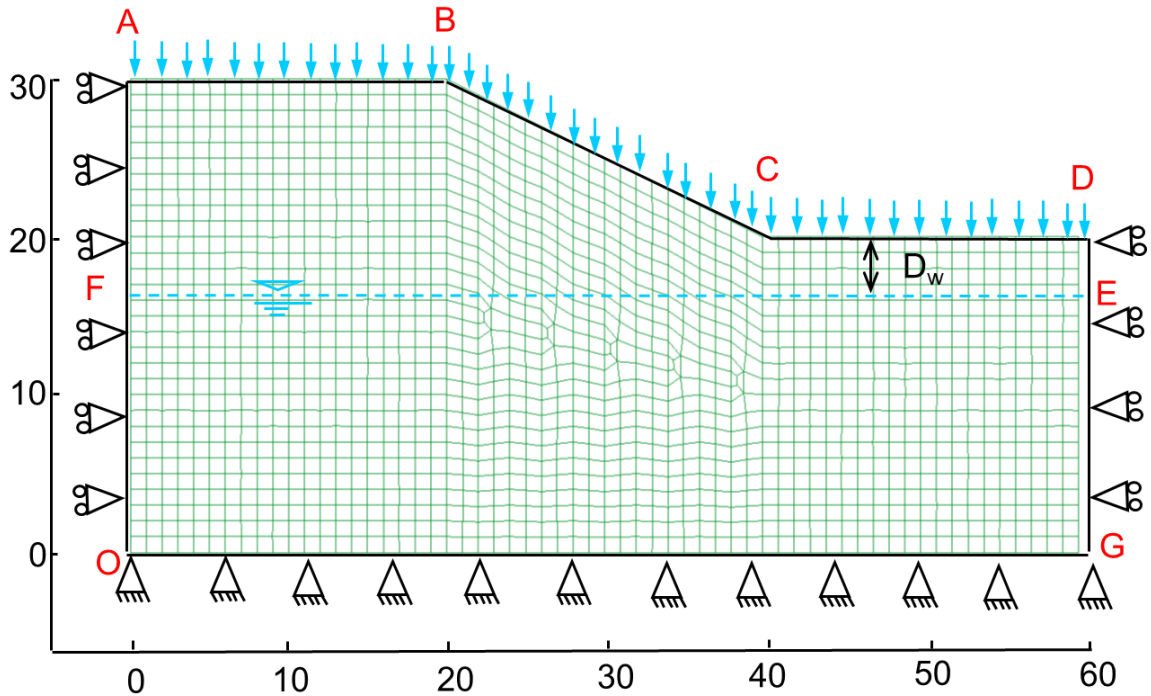


Figure 1: Slope dimensions and boundary conditions (scale in meters)

The numerical model adopted in the present analysis consists of a slope with a 2:1 gradient discretized into a finite element mesh of 1515 quadrilateral elements with four integration point and an average area of $\sim 1\text{m}^2$ (Figure 1). The finite element CODE_BRIGHT software (Olivella et al. 1996; UPC 2010) was adopted to conduct the numerical analyses. This software allows fully coupled thermo-hydro-mechanical simulations of boundary value problems in unsaturated soils. Thermal processes are however not considered in this study, which focuses exclusively on coupled hydro-mechanical processes.

A mesh sensitivity analysis was initially performed under saturated conditions, which confirmed the accurate estimation of the safety factor by the model shown in Figure 1 (Le 2011). The suitability of the mesh was further verified in unsaturated conditions against commercial software (GEO-SLOPE International Ltd) using the limit equilibrium

method. For a given rainfall, the commercial software produced similar changes of the factor of safety compared to the adopted finite element model (Le et al. 2015).

2.2 Hydraulic and mechanical models

The hydraulic constitutive models adopted in this study are presented in Eqs. 1 to 5:

$$S_e = \frac{S - S_r}{S_s - S_r} = \left(1 + \left(\frac{s}{s_e} \right)^{\frac{1}{1-m}} \right)^{-m} \quad (1)$$

$$s_e = s_{eo} \exp(\eta(\phi_o - \phi)) \quad (2)$$

$$k_s = k_{so} \frac{\phi^3}{(1-\phi)^2} \frac{(1-\phi_o)^2}{\phi_o^3} \quad (3)$$

$$k_r = \sqrt{S_e} (1 - (1 - S_e^{1/m})^m)^2 \quad (4)$$

$$\mathbf{q} = -k_s k_r \left(\frac{u_w}{\rho_w g} + z \right) = -k_u \nabla \left(\frac{u_w}{\rho_w g} + z \right) \quad (5)$$

This work employs the van Genuchten (1980) model for the soil water retention curve (SWRC) (Eq. 1-2), the Kozeny's relationship (Kozeny 1927) between saturated permeability and porosity (Eq. 3) and the van Genuchten and Nielsen (1985) model for the unsaturated relative permeability (Eq. 4). The unsaturated permeability k_u is then the product of the saturated and relative permeabilities (i.e. $k_u = k_s k_r$) while the unsaturated flow \mathbf{q} is calculated using the generalised Darcy's law (Eq. 5). The above models can realistically describe unsaturated flow in a simple and numerically stable way, which is highly desirable when dealing with finite element simulations. Nevertheless, they rely on the simplifying assumption that capillarity dominates the hydraulic regime and that other forces linked to adsorptive phenomena are negligible.

The SWRC (Eq. 1) relates the effective degree of saturation S_e to suction s through the air entry suction parameter s_e and the retention gradient m (van Genuchten 1980). The value

of S_e is calculated as a function of the current degree of saturation S , the maximum degree of saturation S_s , and the residual degree of saturation S_r . The effect of heterogeneity is introduced by relating the parameter s_e to porosity ϕ through the parameter η (Eq. 2) that controls the rate at which s_e deviates from its reference value s_{e0} when ϕ deviates from its reference value ϕ_0 (Rodríguez et al. 2007; Zandarín et al. 2009). Similarly, Kozeny's equation (Eq. 3) describes the deviation of the saturated permeability k_s from its reference value k_{s0} when ϕ deviates from its reference value ϕ_0 (Kozeny 1927). The van Genuchten and Nielsen (1985) permeability curve (Eq. 4) relates instead the relative permeability k_r to the effective degree of saturation S_e , and therefore indirectly to porosity ϕ , through the gradient m of the SWRC curve. The symbols u_w , ρ_w , g and z indicate the pore water pressure, the water density, the gravitational acceleration and the elevation coordinate, respectively. The water retention behaviour and permeability are therefore spatially heterogeneous which influences the hydraulic processes within the soil masses. More details about these relationships can be found in UPC (2010).

Unless otherwise stated, the base values of m , k_{s0} , s_{e0} and η are constant and equal to the values shown in Table 1. These values are about the middle of their respective typical range of variation (i.e. those values that are physically possible and are of interest in practically applications) to avoid unrepresentative results (Bear 1972; van Genuchten 1980; Zandarín et al. 2009). The base value of $k_{s0}=10^{-5}$ m/s lies in the upper permeability range of layered clays or clayey silts. The choice of a relatively high k_{s0} facilitates numerical simulations by easing the steep change of pore pressure across the wetting front. During the sensitivity analysis, the parameters k_{s0} , η and m are varied in their typical range to investigate the effect on slope stability. In Eq. 1, the values of S_s and S_r are equal to 1 and 0.01, respectively.

A linear elastic model with an extended Mohr-Coulomb (MC) failure criterion (Eq. 6) is adopted to simulate the mechanical behaviour of the unsaturated soil (Fredlund et al. 1978):

$$\tau = c' + \sigma \tan \phi' + s \tan \phi^b \quad (6)$$

Eq. 6 reflects the dependency of the shear stress at failure τ on net normal stress σ and suction s through the effective friction angle ϕ' , effective cohesion c' and a parameter controlling the increase in shear strength with suction ϕ^b . The cohesive component of strength provided by suction (i.e. the 3rd term in Eq. 6) reduces with decreasing s and becomes zero for a fully saturated soil (i.e. $s = 0$). In reality, the value of ϕ^b has been shown experimentally not to be constant but to decrease with increasing s (Escario and Saez 1986; Gan et al. 1988) starting from ϕ' in saturated conditions. In particular, Gan et al. (1988) suggested that, as the soil desaturates, the value of ϕ^b decreases up to a relatively constant value. For simplicity, however, this study assumes a constant value of ϕ^b .

The assumed values of c' , ϕ' and ϕ^b are typical of clays and are based on those reported by Bishop et al. (1960) for boulder clay and by Gan et al. (1988) for a compacted glacial till. The elastic parameters (i.e. Young's modulus E and Poisson's ratio ν), are also related to typical values observed in clayey soils, and chosen within their respective ranges (Zhu 2014). The variation of porosity may also influence mechanical behaviour, but this aspect is not considered in this study. The mechanical parameters are therefore assumed to be homogeneous (spatially uniform) and are set equal to the values listed in Table 1. This assumption facilitates the investigation of the effect of porosity heterogeneity on the hydraulic behaviour by isolating it from other effects.

A non-associated flow rule with zero dilatancy is assumed, which means that no plastic volumetric strains occur during yielding. Moreover, a viscoplastic integration algorithm is used to update the stress field during plastic loading (Olivella et al. 1996).

Table.1: Base values of soil parameters adopted in the numerical analyses

Hydraulic model			Mechanical model		
Symbol	Units	Value	Symbol	Units	Value
m		0.2	E	kPa x 10^3	100
η		5	ν		0.3
ϕ_o		0.333	ϕ'	°	20
k_{so}	m/s	10^{-5}	c'	kPa	5
s_{eo}	kPa	20	ϕ^b	°	18

As shown in Eq. 6, $\tan\phi^b$ controls the increase in shear stress at failure with suction, which provides an additional source of cohesive strength with respect to the effective cohesion c' . Therefore, when implementing the shear strength reduction technique for estimating the factor of safety (FoS), the same reduction is applied to all strength parameters (c'_{actual} , $\tan\phi'_{actual}$, $\tan\phi^b_{actual}$) to obtain the corresponding values at failure (c'_{fail} , $\tan\phi'_{fail}$, $\tan\phi^b_{fail}$) according to the following definition of FoS for unsaturated soils:

$$FoS = \frac{c'_{actual}}{c'_{fail}} = \frac{\tan\phi'_{actual}}{\tan\phi'_{fail}} = \frac{\tan\phi^b_{actual}}{\tan\phi^b_{fail}} \quad (7)$$

The use of Eq. 7 in conjunction with the FE program `CODE_BRIGHT` has been verified against the Limit Equilibrium Method by using the commercial software `SeepW` and `SlopeW` (GEO-SLOPE International Ltd) and has been shown to produce comparable values of FoS (Le 2011, Le et al. 2015). More details about the application of the shear strength reduction method using `CODE_BRIGHT` can be found in Le (2011) and Le et al. (2015).

2.3 Boundary conditions and simulation process

At the very start of the analysis, gravity is applied to an initially weightless slope to establish the initial stress distribution due to self-weight. The acceleration of gravity is increased from zero to the standard value of 9.8 m/s^2 over a 'fictitious' time (UPC 2010). The random porosity field is introduced prior to applying gravity, so that the initial stress distribution takes into account the variation of the soil unit weight due to material heterogeneity.

The initial distribution of pore water pressure p_w is assumed hydrostatic in equilibrium with the water table. The water table is fixed at 5 m below the slope toe, except for those analyses where the effect of water table depth is investigated. The pore air pressure is assumed constant and equal to the atmospheric pressure (i.e. $p_a=0$) and the suction s is therefore equal to the negative value of the pore water pressure (i.e. $s=-p_w$). The initial suction is therefore largest at the crest of the slope AB and equal to $s_{max}=150 \text{ kPa}$ under hydrostatic conditions. This level of surface suction is typically encountered in arid or semi-arid countries such as Australia (e.g., Cameron et al. (2006)). The assumption of an initially hydrostatic pore pressure distribution ignores the potential presence of evaporation at ground level. This simplification is acceptable in the context of this work, whose objective is to analyse the sensitivity of the stability of unsaturated slopes to different parameters rather than describing the hydrological and failure regimes of a real case.

A rainfall of constant intensity is then applied at the boundary $ABCD$ over 10 days (Figure 1). This boundary condition imposes a constant rate of infiltration into the soil as long as the pore water pressure at the boundary is negative (i.e. as long as suction is positive). If the pore water pressure becomes equal or larger than zero, the boundary condition shifts to a constant zero pore water pressure to avoid the build-up of a hydraulic head at the ground surface. This type of boundary condition is often referred to as a "seepage" boundary condition and is further described in CODE_BRIGHT Users' Manual (UPC 2010) or Le et al. (2012). After 10 days, the rainfall is stopped and the

boundary $ABCD$ is assumed impermeable but the simulation is continued for another 355 days to allow the redistribution of pore water pressure back to a hydrostatic condition. The boundaries OA , OG and GD are assumed impermeable during and after the rainfall, which causes the infiltrated water to accumulate inside the soil domain and the water table to rise. This describes a situation in natural slopes where surrounding soils have low permeability or neighbouring areas have poor drainage capacity (e.g., due to a blocked drain). Such a condition can indeed be critical for slope stability in reality. If evaporation and/or dissipation were allowed, the water table position would be affected depending on the considered assumptions. For example, if high rates of evaporation are assumed the rise of the water table will be strongly affected, leading to an eventual little water accumulation in the slope domain and therefore to a practically stable position of the water table during the rainfall. Then, the changes of the safety factor and size of failure mass during the rainfall would be less than the results obtained in this study. In addition, the values of these parameters after the rainfall would be almost the same as at the beginning of the rainfall. Similar reasoning can be used with respect to the inclusion of dissipation in the simulations. The mechanical boundary conditions are also indicated in Figure 1.

The Monte Carlo analysis involves the generation of multiple random porosity fields that are mapped onto the FE mesh shown in Figure 1. These FE meshes with different random porosity fields constitute the “realisations” of the Monte Carlo analysis. Each realisation is analysed in two consecutive stages corresponding to: *i*) the calculation of the pore water pressure and stress fields at distinct times during or after the rainfall; and *ii*) the application of the shear strength reduction technique (SRT) to the calculated pore water pressure and stress fields to determine the factor of safety (FoS) and sliding area (A_s) at a given time.

Note that, in stage *i*), soil deformations are fully coupled with pore water flow and the equations of equilibrium and hydraulic continuity are solved simultaneously in $CODE_BRIGHT$. The nonlinear equations associated with flow and mechanical problems are solved in a fully coupled manner using the New-Raphson method (Olivella

et al., 1996). This implies that as the rainfall seeps into the unsaturated soil, suction (and/or positive pore water pressure) changes will induce net (or effective) stresses changes. This in turn induces deformations in the soil elements. These deformations cause changes in the soil porosity, which lead to changes in intrinsic permeability and air entry value through equations 2 and 3, respectively. The new permeability and air entry value influence the water flows through equation 1, 4 and 5. The unsaturated/saturated flow and the mechanical deformations are therefore truly coupled.

Eight points in time are selected to extract the corresponding fields of stresses and pore water pressure to be used in the subsequent shear strength reduction stage. These include four times during the rainfall (i.e. 0, 0.5, 5, 10 days) and four times after the rainfall (i.e. 15, 20, 100 and 365 days). The selected times aim at capturing the changes in the failure mechanism associated with a significant variation of the pore water pressure p_w field.

Note that the *SRT* analysis is simply a numerical technique used in stage *ii*) to estimate the factor of safety FoS and sliding area A_s corresponding to the field of stresses and pore water pressures calculated at a given time. During a *SRT* analysis, the calculated pore water pressures field is fixed at every mesh node while the calculated stresses and strains fields are imposed as initial conditions. The shear strength parameters are then reduced by a factor that is initially equal to one and subsequently augmented in steps of 0.01 until failure. Failure corresponds to the detection of significant movements on the slope surface. The value of the reduction factor at this point is assumed to coincide with the FoS of the slope (Eq. 7). Note that the above methodology allows the natural development of the slip surface through the weakest path within the soil domain, which is an advantage compared with limit equilibrium methods where the shape of the slip surface is instead assumed. Le et al. (2015) provided detailed explanation of the criteria used to detect the failure mechanism.

After failure, the number of mesh nodes that have moved substantially is counted to compute the sliding area of the slope (Le et al. 2015). One node corresponds to a region that is the sum of one quarter of each of the four elements sharing that node. Since the

mesh mostly consists of square or parallelogram elements of 1 m^2 (Figure 1), the area allocated to each node is approximately 1 m^2 and the number of “failed” nodes provides a reasonably good estimation of the sliding area A_s in m^2 . This is clearly an approximation because the nodes on the boundary of the failed region contribute less area than the inner nodes. Nevertheless, this approximation is considered acceptable as the present study focuses on a sensitivity analysis rather than on the accurate determination of the sliding area. For real slopes, it is recommended that A_s is estimated more accurately either by using a finer mesh or by directly measuring the area of the failed region.

3 Random porosity field

Porosity ϕ is probably one of the most easily measured soil parameters exhibiting spatial variability (Le et al. 2013). Porosity values are theoretically bounded between 0 and 1, thus they should be represented by a bounded random distribution such as the tanh-bounded function. This distribution requires 4 parameters which are a lower bound, an upper bound, the location parameter (equal to 0 when random variable is symmetric about the midpoint of the variable range) and a scale parameter which increases with increasing level of variability. The bounded distributions are mathematically complex so a different approach is employed in the present work by generating an univariate random field of void ratio e instead of porosity ϕ . The void ratio can take any positive value and may thus be modelled by a log-normal probability function (Baecher and Christian 2003; Lacasse and Nadim 1996). The generated random field of void ratio is then converted back into a random field of porosity by using the relationship $\phi=e/(1+e)$. This equation implies that the random field does not generate any value of porosity equal to zero. Such a value is considered unrealistic for the size of the mesh considered in this study.

Random fields of void ratio are produced by using the Local Average Subdivision (LAS) algorithm and the Markov auto-correlation function (Fenton 1990). The Local Average Subdivision (LAS) method (Fenton, 1990) involves a recursive subdivision process. The original domain is first subdivided into equal sized area, then each area is divided again into smaller areas and this process keeps going until the desirable resolution is achieved.

At every stage of subdivision, random values are generated for each area with the variance and covariance structure inherently related to the size of the subdivided area relative to the original domain. Both the LAS algorithm and the Markov function have already been used in geotechnical engineering (Fenton 1990; Griffiths and Fenton 2004). The random field is generated over a regular grid covering a rectangular area with dimensions equal to the largest width and height of the soil domain. The grid is then superimposed on the finite element mesh, so that the bottom left corners of the grid and mesh coincide. An algorithm is subsequently executed to identify the cell in the random field grid with the closest centroid to the centroid of each finite element. The void ratio of the finite element is then taken to coincide with the random value of that cell. Le (2011) explains in detail the procedure to verify that statistical parameters are correctly transferred in the above mapping process.

The effect of the statistical parameters governing the random distribution of void ratio e (i.e. mean $\mu(e)$, standard deviation $\sigma(e)$ and correlation length $\theta(e)$) were studied in detail in Le et al. (2015). In this study, the values of the mean $\mu(e)$, coefficient of variation $COV_e = \sigma(e)/\mu(e)$ and correlation length $\theta(e)$ are therefore kept constant and equal to 0.5, 0.8 and 8 m, respectively (which correspond to $\mu(\phi) = 0.3$, $COV_\phi = 0.46$ and $\theta(\phi) = 8$ m). The effect of COV_e and $\theta(e)$ has been investigated in another study (Le et al. 2015). The chosen values for COV_e and $\theta(e)$ aim to avoid too large or too small effect of these parameter on the results, and increase the possibility of observing the effect of porosity heterogeneity on suction distribution within the slope.

Figures 2a and 2b show the influence of porosity on the SWRC and k_u curves calculated using Eqs. 1-4 and the input parameters are listed in Table 1. Six values of porosity, from 0.05 to 0.8, are considered. A value of porosity outside this range is quite unlikely considering the coefficient of variation adopted in this study. Based on Figure 2a, the initial degree of saturation near the crest of the slope (i.e. $s \approx 150$ kPa) varies between 0.3 and 0.8 with a corresponding value of k_u in the range 10^{-10} – 10^{-9} m/s.

A heterogeneous porosity field therefore generates non-uniform distributions of degree of saturation and permeability (in addition to a non-uniform distribution of specific weight), which leads to an irregular advancement of the wetting front and an uneven distribution of pore water pressures. This affects the distribution of shear strength, which is controlled by pore water pressure (in addition to the distribution of stresses, which is governed by the overburden weight) and has an impact on the factor of safety of the slope as well as on the size of the sliding mass.

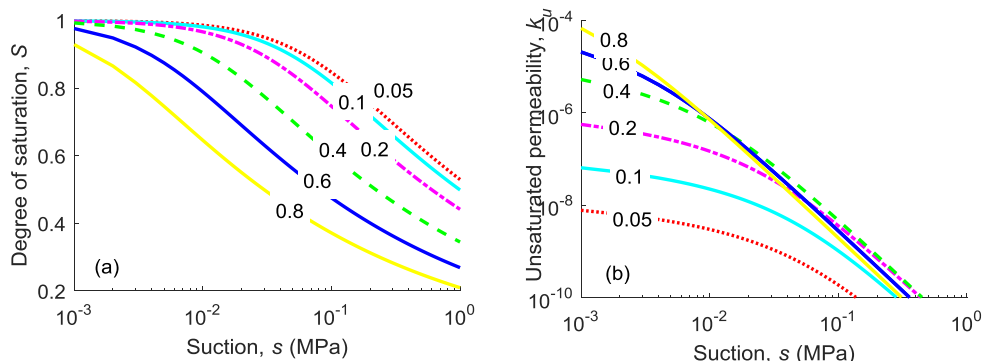


Figure 2. Influence of porosity on the variation of degree of saturation (a) and unsaturated permeability (b) with suction.

Noticeably, the degree of saturation (Figure 2a) decreases with increasing porosity while the unsaturated permeability (Figure 2b) increases with increasing porosity. The latter (i.e. k_u) is however little affected when suction is above 20 kPa and the porosity is higher than 0.2. This implies that, in unsaturated soils, the higher porosity regions are not necessarily the most permeable ones, as it is instead the case in saturated soils.

4 Influence of hydraulic characteristics

4.1 Water table depth

The initial suction of the soil affects both its degree of saturation and unsaturated permeability (Eqs. 1 and 4), which makes the initial position of the water level (D_w) an important factor to consider. Three values of water table depth measured with respect to

the toe of the slope are investigated in this section, namely 0, 5 and 10 m. Under hydrostatic conditions, these depths correspond to the three maximum values of initial suction at the crest of the slope of 100, 150 and 200 kPa, respectively. For each depth, two analyses are compared: one considering the effect of suction on shear strength, i.e. $\phi^b=18^\circ$, and one neglecting this effect, i.e. $\phi^b=0$.

The evolution of the mean and coefficient of variation of FoS , i.e. $\mu(FoS)$ and COV_{FoS} , are presented in Figures 3a and 3b, respectively. When the effect of suction is considered (i.e. $\phi^b=18^\circ$), the $\mu(FoS)$ progressively decreases during the rainfall, because of the reduction in shear strength triggered by the reduction of suction in the unsaturated region but also because of the build-up of positive pore water pressures in the saturated area at the slope toe. In all the analyses, the lowest value of $\mu(FoS)$ occurs just before the end of the rainfall. The $\mu(FoS)$ then recovers over the post-infiltration period (i.e. day 10 to 365), because of the suction increase caused by the downward drainage and the consequent dissipation of positive pore water pressure. The final $\mu(FoS)$ values (i.e. at day 365) are lower than the initial ones because of the rise of water table induced by the accumulation of infiltrated water.

For the case of $\phi^b=18^\circ$, the $\mu(FoS)$ consistently increases with increasing D_w because of the increase in shear strength with growing suction. As rainfall progresses, the slope with the deepest initial water table (i.e. $D_w=10$ m) loses the largest amount of suction, leading to the most substantial reduction in $\mu(FoS)$ from about 2.4 to 1.3 over the 10 days of the rainfall. Instead, the $\mu(FoS)$ of the slope with the shallowest initial water table (i.e. $D_w=0$ m) reduces much less from about 1.3 to 1.0 over the same time.

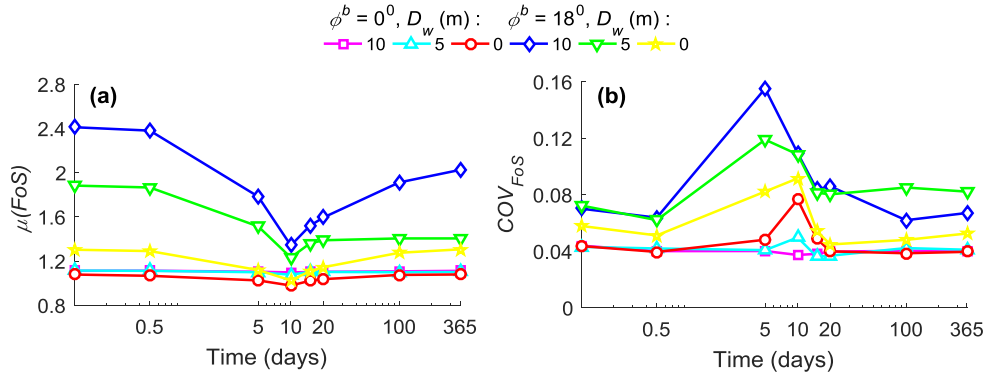


Figure 3: Time evolution of FoS in terms of mean (a) and coefficient of variation (b). Analyses: influence of water table depth D_w .

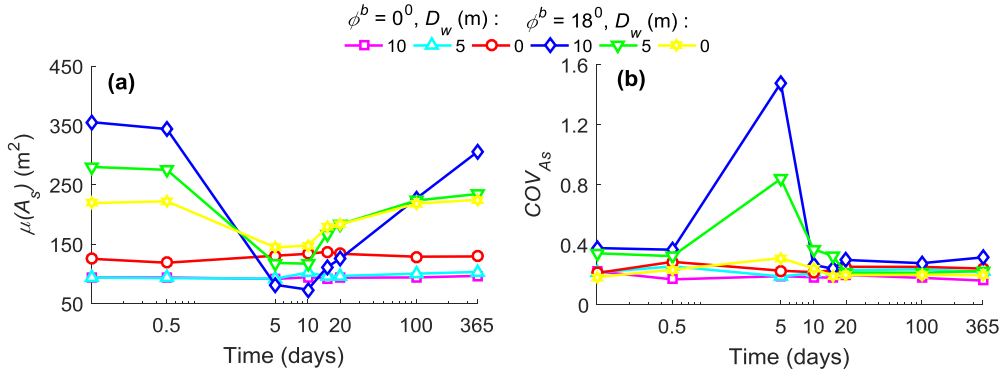


Figure 4. Time evolution of A_s in terms of mean (a) and coefficient of variation (b). Analyses: influence of water table depth D_w .

Similar results are shown in Figures 4a and 4b but in terms of $\mu(A_s)$ and COV_{A_s} , respectively. When the effect of suction is included ($\phi^b=18^\circ$), the value of $\mu(A_s)$ consistently decreases during the rainfall (though at different rates depending on the D_w value) and reaches a plateau between 5 and 10 days before increasing again during the post-infiltration period. The reason behind this behaviour is that, at the start of the rainfall, the shallow soil region exhibits considerable strength arising from the high suction, which 'pushes' the slip surface to deeper layers in the search of a 'weak' path (Figure 5). However, after a rainfall time between 5 and 10 days, the shallow soil experiences a dramatic loss of suction and therefore becomes significantly weaker than the deeper soil. This in turn promotes the formation of a slip surface through the wetted shallow soil layer, which explains why A_s tends to decrease (Figure 5b, 5d, 5f).

For the case of $\phi^b=18^\circ$, the values of $\mu(A_s)$ are higher for larger values of D_w , both at the beginning (i.e. 0 to 0.5 day) and at the end (i.e. 100 to 365 days) of the analysis, because of the larger soil suction associated to a depressed water table (Figure 5a, 5c and 5e). During the course of the rainfall, the wetted area decreases in depth with increasing D_w because of the higher initial suction, and hence the lower degree of saturation and permeability, which delays water infiltration (Figure 5b, d and f). This explains the higher value of $\mu(A_s)$ with smaller D_w between 5 and 10 days (Figure 4a).

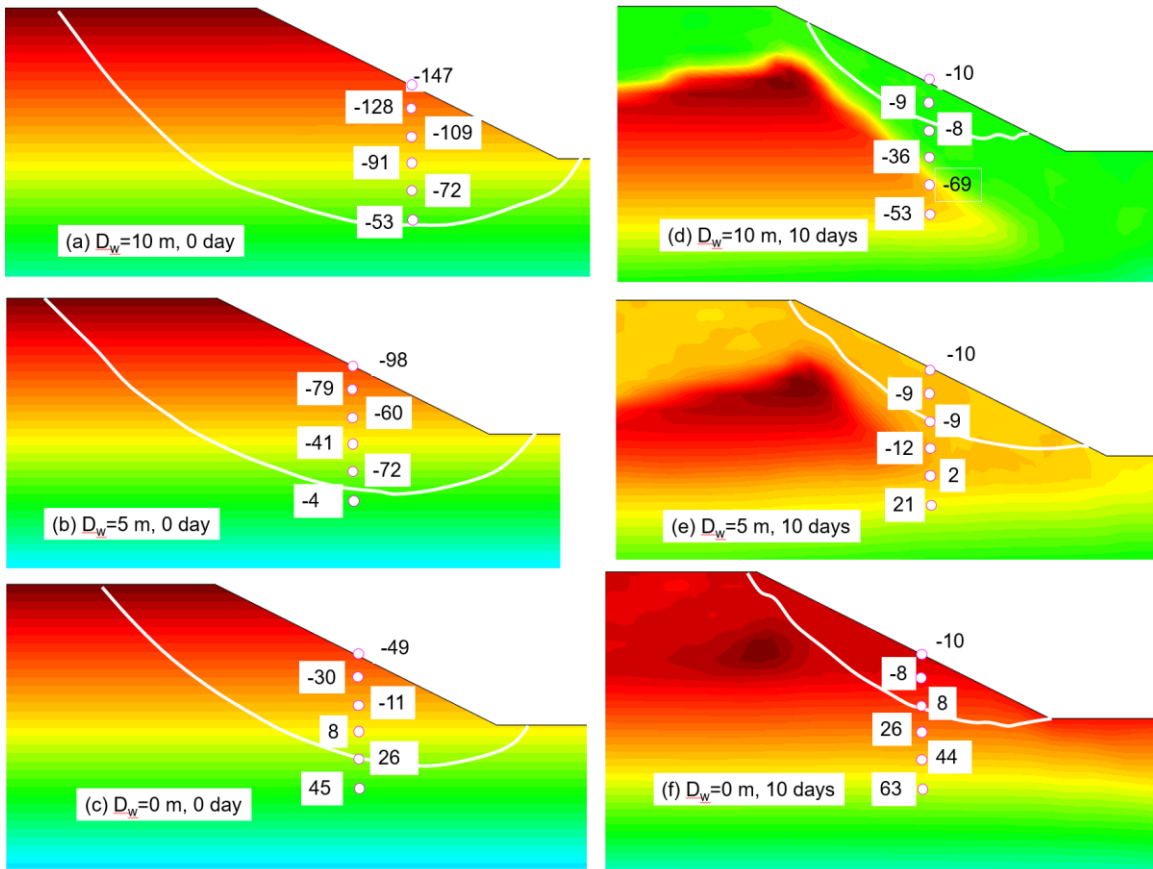


Figure 5. Contour maps of p_w and slip surfaces for different D_w at different times ($\phi^b=18^\circ$). The p_w values shown in labels are in kPa. The p_w colour scale is not the same for all contour plots.

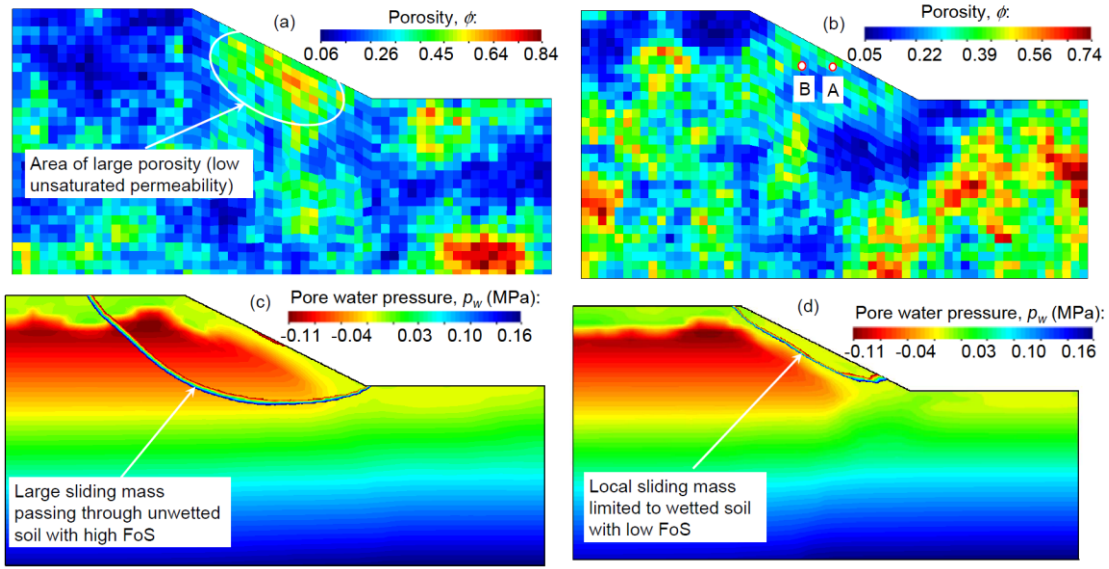


Figure 6: Porosity distributions of sample realisations with significantly different failure mechanisms (a, b) and contour maps of p_w with sliding surfaces at 5 days (c, d). Results correspond to $\phi^b=18^\circ$ and $D_w=5$ m.

For the case of $\phi^b=18^\circ$, the sliding area at 5 days varies over a wide range of values depending on the depth of the wetting front in each realisation. There appears to be a 'critical' depth such that, when the wetting front moves below it, the sliding area is confined to the superficial wetted region (Figure 6b and 6d). In this case, the FoS tends to be low, because the suction of the 'wetted' elements is relatively low (Figure 56d). Conversely, if the wetting front is shallower than the 'critical' depth, the slip surface tends to be deep seated (Figure 6c), like at the start of the rainfall, with a large FoS due to the high suction along the slip surface. This case might correspond to the existence of a low permeability layer that prevents the advancement of the wetting front (Figure 6a). The equal occurrence of both these two extremes (i.e. shallow versus deep slip surfaces) causes the large values of COV_{FoS} and COV_{As} at 5 days. At 10 days, the wetting front is likely to have passed the 'critical' depth and hence the majority of slip surfaces is confined to the superficial wetted region, which explains the consistent decrease in COV_{FoS} and COV_{As} . An exception to this behaviour is the COV_{FoS} for the case of $D_w=0$ m,

which peaks at 10 days because of the dominant destabilizing effect of positive pore pressure build-up at the slope toe.

The peak values of COV_{FoS} and COV_{A_s} significantly increase with increasing D_w implying that the factor of safety and the size of the sliding area become more variable between realisations. After the peak, the values of COV_{FoS} and COV_{A_s} decrease because of water drainage causing an increase of suction in the unsaturated region and a dissipation of positive pore pressures in the saturated region, which reduce the difference between realisations.

When the effect of suction on shear strength is not considered (i.e., $\phi^b=0$), Figure 3 shows that the $\mu(FoS)$ is virtually constant for all three D_w values, with only a slight decrease at day 10 for $D_w=0$, while the COV_{FoS} increases slightly with decreasing D_w between 5 and 20 days. The build-up of positive pore water pressures with decreasing D_w is the main reason behind this trend given that a larger portion of the slip surface passes through the saturated region as the initial water table is shallower. Figure 4 shows that $\mu(A_s)$ and COV_{A_s} remain fairly constant over time. Inspection of displacement contours (not shown here) reveal that the sliding areas are very similar for $D_w=5$ m and $D_w=10$ m and do not practically change over time. When the water table is at the ground surface, sliding areas tend to be slightly larger due to the additional stabilizing effects provided by the weight of water in the saturated part of the slope.

Similar patterns of variation with time of the mean and coefficient of variation of both FoS and A_s were observed in all cases hereafter, hence they will not be discussed further. The comments will instead focus on the sensitivity of the results to the parameters under study.

4.2 Saturated permeability

The reference saturated permeability k_{so} controls the infiltration rate and influences the advancement of the wetting front together with the distribution of pore water pressures. A range of realistic k_{so} values, from 10^{-4} m/s (e.g. pervious well sorted sands) to 10^{-7} m/s

(e.g. silts or layered clays), is investigated in this section to gain insights into the influence of this parameter on slope stability.

Figure 7 and Figure 8 show similar variations of $\mu(FoS)$, $\mu(A_s)$, COV_{FoS} and COV_{A_s} over time as observed in the previous section, except for the lowest value of the reference permeability (i.e. $k_{so}=10^{-7}$ m/s). In this case, almost no water infiltrates the soil and all curves remain practically flat over the entire simulation period.

Notably, the variation of $\mu(FoS)$ and COV_{FoS} with k_{so} is not monotonic (Figure 7) and the intermediate value of k_{so} (i.e. 10^{-5} m/s) causes the largest average drop of factor of safety as well as the widest variability between realisations (i.e. lowest $\mu(FoS)$ and highest COV_{FoS} for the period 5 to 10 days). This is because the highest value of k_{so} (i.e. 10^{-4} m/s) facilitates water flow leading to smaller gradients of pore pressure together with smaller drops in suction, which results in smaller reductions of shear strength. Conversely, the intermediate value of k_{so} (i.e. 10^{-5} m/s) generates larger gradients of pore pressure with bigger suction drops, which allows the sliding surface to remain inside the wetted region at the surface. This explains the lower values of $\mu(FoS)$ and $\mu(A_s)$ and the higher values of COV_{FoS} and COV_{A_s} for $k_{so}=10^{-5}$ m/s compared to $k_{so}=10^{-4}$ m/s. The evolution of pore water pressures at the two sampling points shown in Figure 9a confirms the larger suction drops at 10 days for $k_{so}=10^{-5}$ m/s compared to $k_{so}=10^{-4}$ m/s (Figure 10).

The lower value of k_{so} (i.e. 10^{-6} m/s) limits infiltration and restricts the water movement to a very shallow layer along the slope face (Figure 9b). In this case, most of the suction loss is limited to the narrow top region (Figure 10a) while a wider wetted region develops at the slope toe (Figure 9b). Slip surfaces concentrate in this wetted region, which results in smaller values of COV_{FoS} with higher values of $\mu(FoS)$ compared to the previous two cases (Figure 7). Moreover, the value of $\mu(A_s)$ shows a sharp drop at 10 days because of the dominant failure mode cutting through the wetted region above the slope toe (Figure 8a). The COV_{A_s} attains a sharp peak at 10 days (Figure 8b) because of the contrast between the majority of realisations predicting a small sliding area constrained to the wetted region and few others predicting a very large value of the sliding area. The latter

scenario is observed when the area near the slope toe is dominated by highly permeable soil.

The drop of $\mu(A_s)$ and the peak of COV_{A_s} appear earlier (i.e. around 5 days) for the case of $k_{so}=10^{-5}$ m/s compared to the case of $k_{so}=10^{-6}$ m/s. This is because the soil with $k_{so}=10^{-5}$ m/s is permeable enough to allow the rapid advancement of the wetting front normal to the slope face. Instead, in the case of $k_{so}=10^{-6}$ m/s, the narrow water path parallel to the slope face requires a longer time to accumulate enough water at the toe slope for inducing failure.

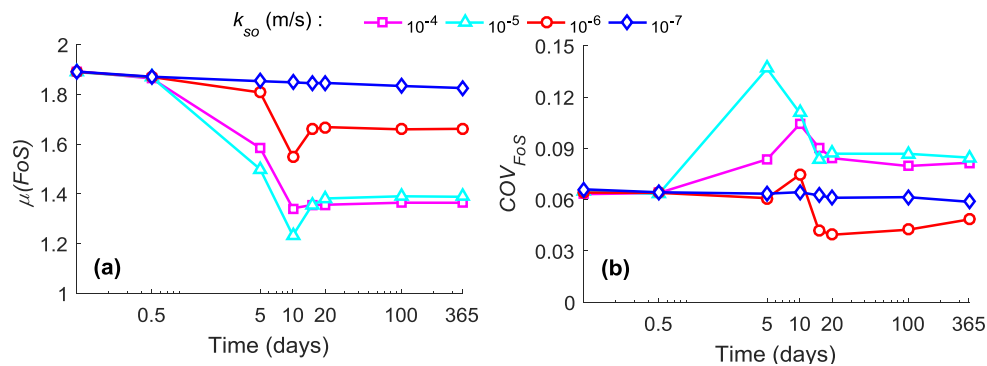


Figure 7. Time evolution of FoS in terms of mean (a) and coefficient of variation (b).
Analyses: influence of reference saturated permeability k_{so} .

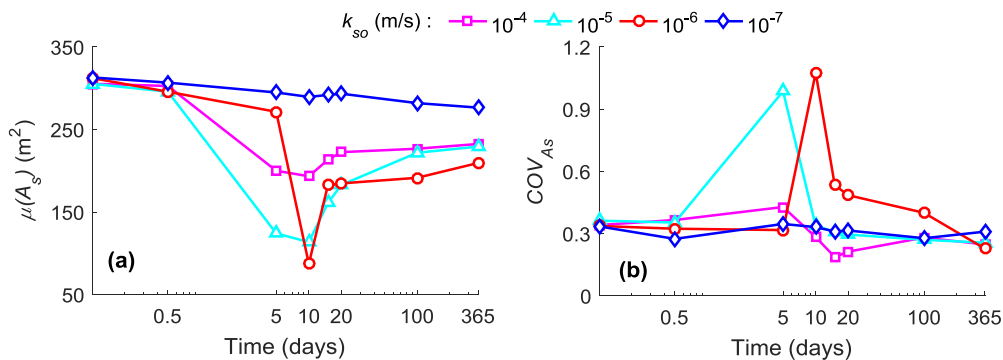


Figure 8. Time evolution of A_s in terms of mean (a) and coefficient of variation (b).
Analyses: influence of reference saturated permeability k_{so} .

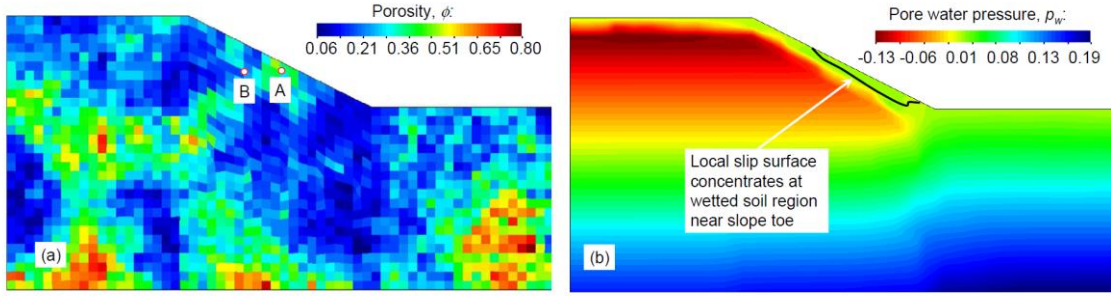


Figure 9. Porosity distribution of a sample realisation showing sampling points (a) and contour map of p_w with slip surface at 5 days for the case of $k_{so}=10^{-6}$ m/s (b).

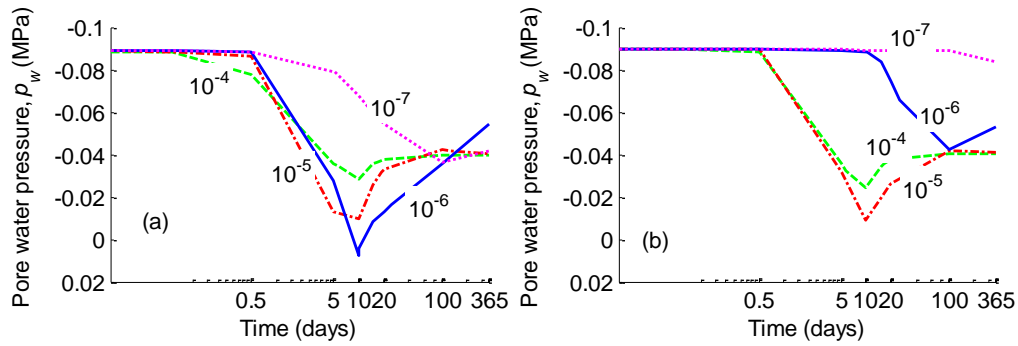


Figure 10. Time evolution of p_w for different values of the reference saturated permeability k_{so} at sampling points A (a) and B (b). Results correspond to the porosity distribution and sampling points shown in Figure 9a.

4.3 Rainfall intensity

The rainfall intensity I_r affects both the amount and rate of water infiltrating into the soil. To investigate this aspect, five rainfalls of different intensities, from very light (i.e. $I_r=4.32$ mm/day) to extremely heavy (i.e. $I_r=432$ mm/day), are applied to each realisation in five separate finite element simulations.

As expected, the suction drop is more significant for the heavier rainfalls as the amount of water supply is larger (Figure 11). Therefore, the value of $\mu(ForS)$ generally decreases with increasing I_r with the most noticeable differences between 5 to 20 days (Figure 12a).

The two lighter rainfalls (i.e. $I_r=4.32$ and 8.64 mm/day) do not provide enough water to induce a substantial change of soil suction, hence the values of $\mu(FoS)$, $\mu(A_s)$, COV_{FoS} and COV_{A_s} remain approximately constant over time (Figure 12 and Figure 13).

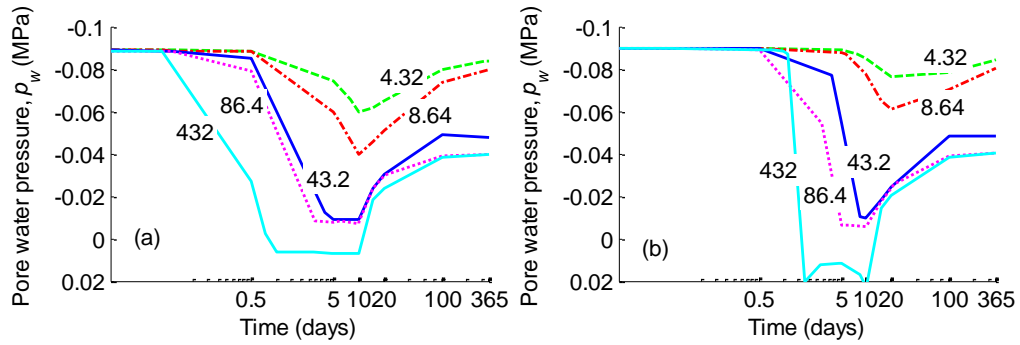


Figure 11. Time evolution of p_w for different rainfall intensities I_r at sampling points A (a) and B (b). Results correspond to the porosity distribution and sampling points shown in Figure 9a.

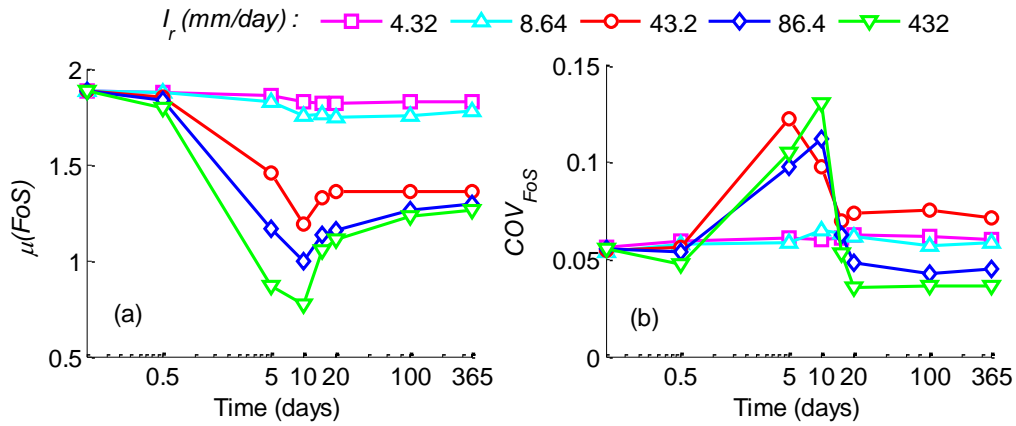


Figure 12. Time evolution of FoS in terms of mean (a) and coefficient of variation (b). Analyses: influence of rainfall intensity I_r .

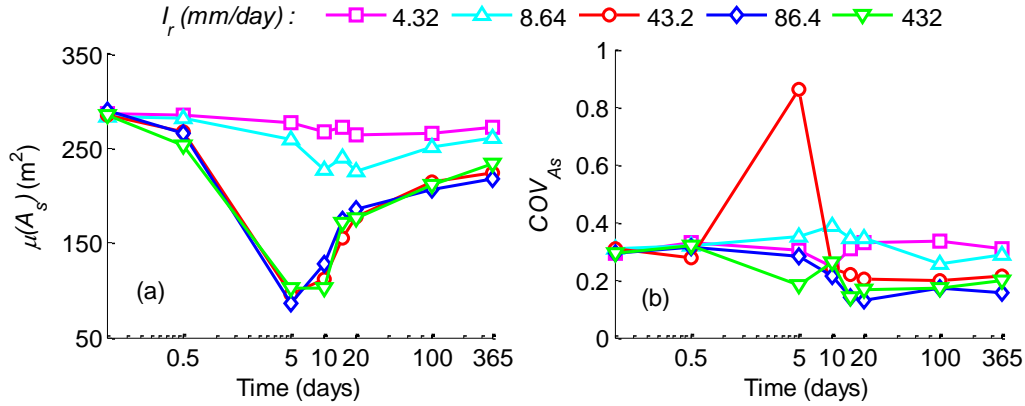


Figure 13. Time evolution of A_s in terms of mean (a) and coefficient of variation (b). Analyses: influence of rainfall intensity I_r .

4.4 Soil water retention curve – Parameter η

The parameter $\eta > 0$ controls the dependency of the air entry value s_e (Eq. 2) on porosity and therefore influences the variation of both degree of saturation S (Eqs. 1 and 2) and unsaturated permeability $k_u = k_r k_s$ (Eqs. 1, 2 and 4) with porosity. Figure 14 shows the variation of degree of saturation S and unsaturated permeability k_u with porosity ϕ at a reference suction $s = 100$ kPa for four different values of η , namely $\eta = 0, 5, 10$ and 15 . The non-monotonic variation of unsaturated permeability k_u (Figure 14b) is the result of the competition between the growth of saturated permeability k_s (Eq. 3) and the reduction of relative permeability k_r (Eq. 4) with increasing porosity ϕ . For $\eta = 0$, however, the variation of unsaturated permeability k_u with porosity ϕ is exclusively governed by the saturated permeability k_s as the degree of saturation S , and hence the relative permeability k_r , are independent of porosity. This explains the monotonic variation of k_u for the particular case where $\eta = 0$ (Figure 14b).

In Figure 14, the curves for different values of η cross each other at the reference porosity ϕ_o , which means that for $\phi > \phi_o$ the degree of saturation S and the unsaturated permeability k_u increase with increasing η while the opposite is true for $\phi < \phi_o$.

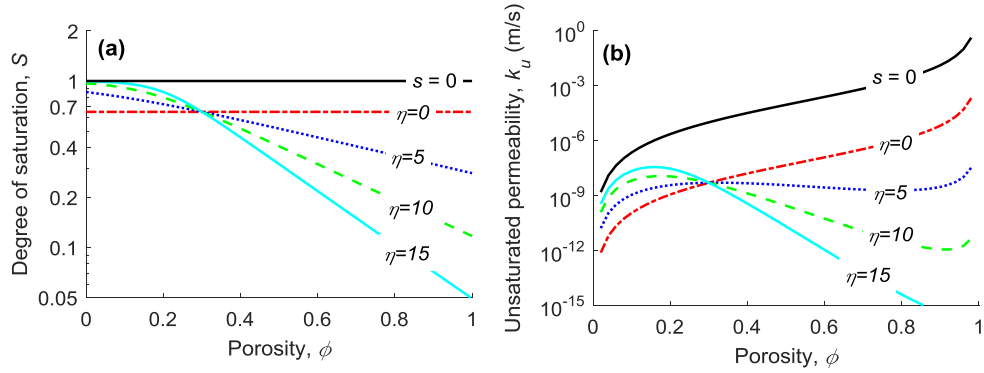


Figure 14. Variation of S (a) and k_u (b) with η at a reference suction $s=100$ kPa. For the saturated case (i.e. $s=0$), S and k_u are independent of η .

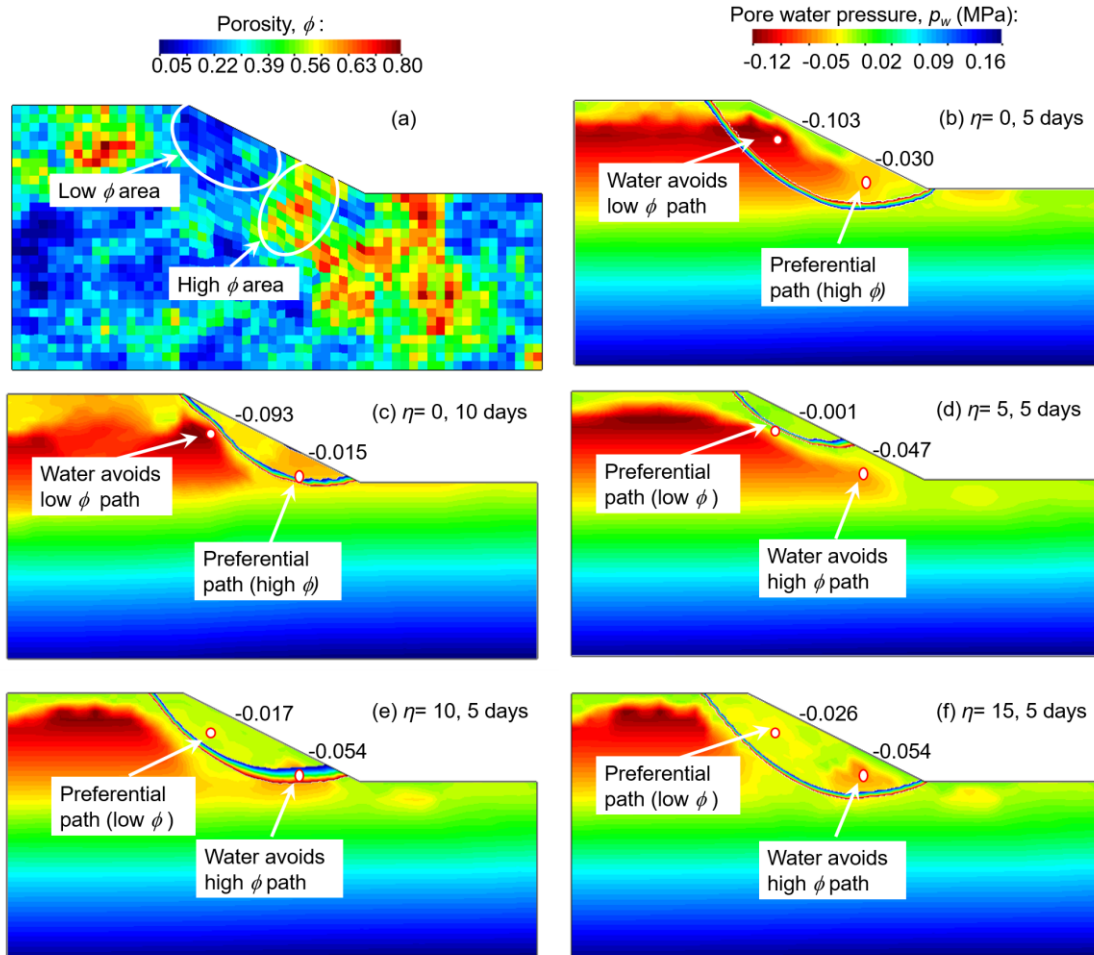


Figure 15. Porosity distribution of a sample realisation (a) and corresponding contour maps of p_w with slip surfaces at different times and for different η values (b, c, d, e, f).

For $\eta=5, 10$ or 15 , the reduction of suction caused by rainfall infiltration is more significant in the low porosity regions (i.e. in the upper part of the slope for the realisation shown in Figure 15a) than in the high porosity ones (Figures 15d, 15e, 15f) while the opposite is true for $\eta=0$ (Figures 15b, 15c). This is because, when $\eta=5, 10$ or 15 , the water preferentially flows through low porosity regions, i.e. those regions where $\phi < \phi_o$, due to their higher unsaturated permeability (Figure 14b). The opposite is true for the case where $\eta=0$.

Figure 16a shows the variation of $\mu(FoS)$ with time, which is almost identical for the three cases where $\eta=5, 10$ or 15 and significantly bigger for the case where $\eta=0$. This pattern is justified by the fact that, in the absence of coupling between porosity and air entry value (i.e. $\eta=0$), water flows preferentially through the higher porosity regions, which require longer times to become saturated. This delays the advancement of the wetting front and explains the higher values of $\mu(FoS)$ for $\eta=0$ compared to $\eta=5, 10$ or 15 . The values of COV_{FoS} are also relatively similar for the three cases where $\eta=5, 10$ or 15 but significantly smaller for the case where $\eta=0$ (Figure 16b).

In terms of sliding area, the value of $\mu(A_s)$ decreases with decreasing η , except for the case where $\eta=0$, which exhibits the highest value of $\mu(A_s)$ at 5 days due to the delayed advancement of the wetting front (Figure 17a). The unsaturated permeability k_u exhibits the weakest dependency on porosity ϕ for the case where $\eta=5$ (Figure 14) leading to similar reductions of suction in the superficial wetted region regardless of whether porosity is high or low. This also explains why, in the case of $\eta=5$, suction is lower and full saturation of the top layer is reached at around 5 days (Figure 15d), leading to the formation of smaller sliding areas, i.e. lower values of $\mu(A_s)$ and higher values of COV_{A_s} (Figure 17 b).

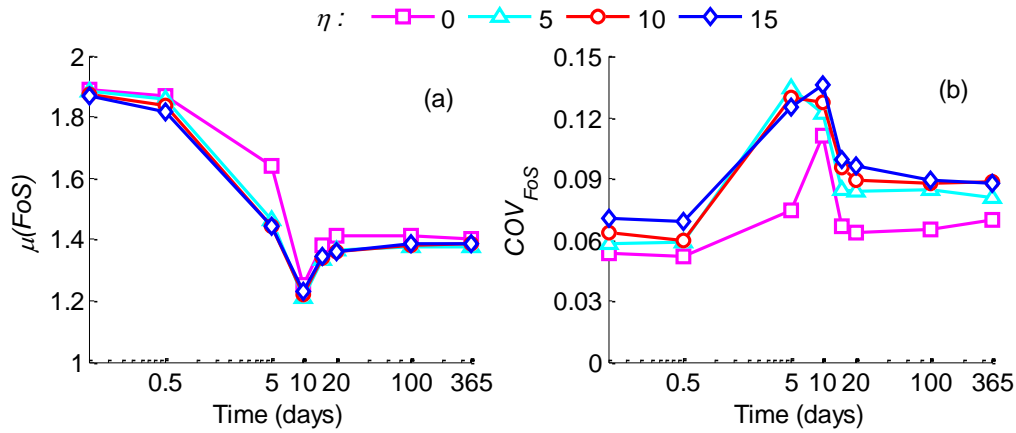


Figure 16. Time evolution of FoS in terms of mean (a) and coefficient of variation (b).
Analyses: influence of the SWRC (parameter η).

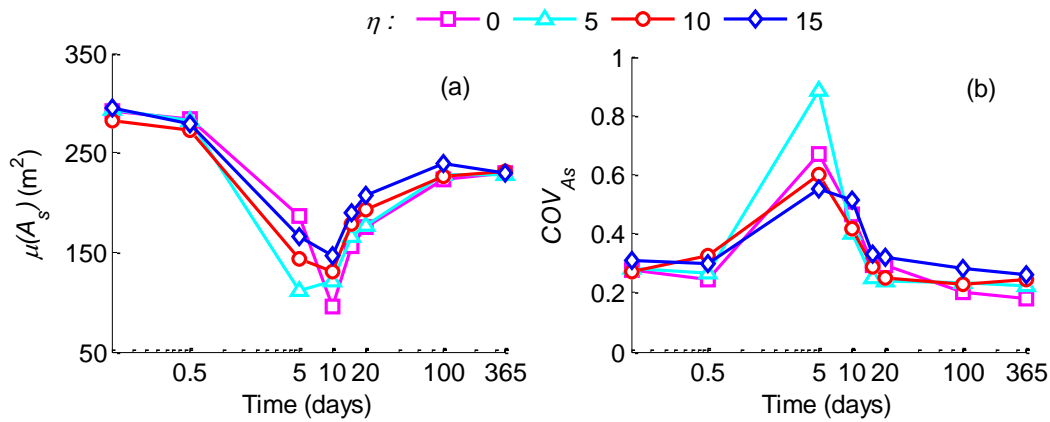


Figure 17. Time evolution of A_s in terms of mean (a) and coefficient of variation (b).
Analyses: influence of the SWRC (parameter η).

4.5 Soil water retention curve – Parameter m

The slope of the water retention curve (Eq. 1) becomes more pronounced as the value of parameter m increases, which results in a decrease of degree of saturation and unsaturated permeability at a given suction (Eqs. 1 and 4). Figure 18 shows the variation of degree of saturation S and unsaturated permeability $k_u = k_r k_s$ with porosity ϕ at a reference suction $s = 100$ kPa for four different values of m , namely $m = 0.05, 0.1, 0.2, 0.4$ and 0.8 . The variation of k_u with ϕ is relatively modest for $m \leq 0.4$ because of the competing effects of

the increase of saturated permeability k_s (Eq. 3) and the decrease of relative permeability k_r (Eq. 4) with increasing porosity ϕ .

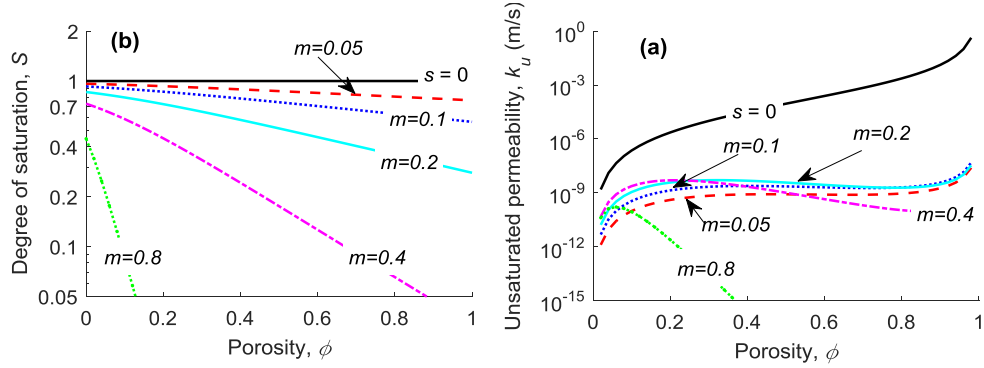


Figure 18: Variation of S (a) and k_u (b) with m at a reference suction $s=100$ kPa. For the saturated case (i.e. $s=0$) S and k_u are independent of m .

For a given porosity, if the value of m is small, the soil exhibits a high initial value of S and therefore requires less water to reach the saturated state (Figure 18a). This produces a quicker advancement of the wetting front so that an earlier and larger reduction of suction occurs in the superficial soil layer as shown in Figure 19. This in turn causes an earlier a larger reduction of shear strength, which explains why at the end of the rainfall (i.e. 10 days) the value of $\mu(FoS)$ is about 1.6 for $m=0.8$ but less than 1 for $m=0.05$ (Figure 18a).

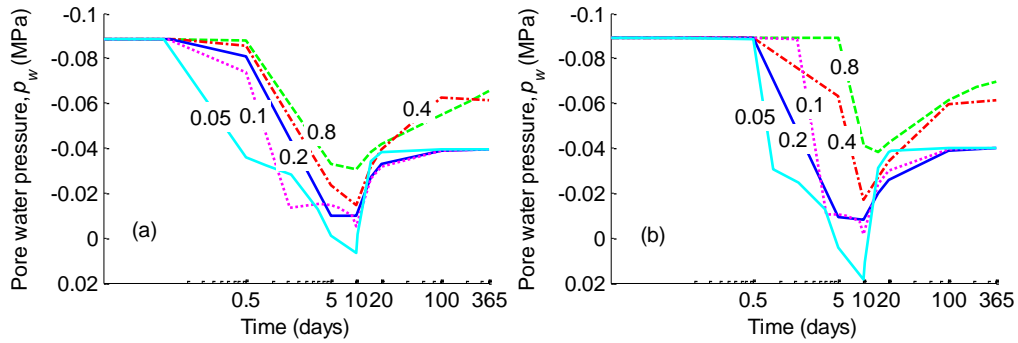


Figure 19. Time evolution of p_w for different values of parameter m at sampling points A (a) and B (b). Results correspond to the porosity distribution and sampling points shown in Figure 6b.

In Figure 20b, the value of COV_{FoS} increases with increasing m at initial times (i.e. between 0 and 0.5 day) because of the increasing variability in overburden weight. However, the highest COV_{FoS} is achieved at 5 days for an intermediate value of $m=0.2$,

which produces the largest spread of failure mechanisms (e.g. Figure 6c and Figure 6d). This is also reflected in the relatively large value of COV_{A_s} . For the larger value $m = 0.4$, the value of COV_{FoS} peaks at 10 days instead of 5 days due to the slower migration of the wetting front compared to the case of $m = 0.2$ as discussed earlier. Similarly, the magnitude of the peak is smaller because most realisations have not reached yet the critical depth. For the smaller values $m = 0.05$ and 0.1 , the wetting front advances faster and is likely to have already passed the critical depth at 5 days. At this time, the vast majority of realisations therefore exhibit sliding areas confined to the top wetted region and correspond, on average, to lower values of FoS and A_s . In this case, the peak of COV_{FoS} at 10 days is caused by the development of a different failure mechanism caused by the rise of the water table in a considerable number of realisations. This higher water table produces the build-up of positive pore pressures and the formation of slip surfaces cutting through the deep saturated region.

As for the largest value $m = 0.8$, the COV_{FoS} uncharacteristically drops to the lowest value at 10 days (Figure 20b). This is probably due to the fact that the rainfall infiltration reduces the initially large non-uniformity of overburden weight in the unsaturated zone.

The value of $\mu(A_s)$ decreases during the rainfall with the lowest values recorded between 5 days for $m = 0.1$ and 10 days for $m = 0.05, 0.2, 0.4$ and 0.8 (Figure 21a). The values of $\mu(A_s)$ for $m = 0.4$ and 0.8 are generally higher than in all other cases because the wetting front did not reach the critical depth in the majority of realisations, which means that the factor of safety and sliding area are generally large.

The variation of A_s between realisations is marginal for small values of m (i.e. 0.05 and 0.1) with no prominent peaks of COV_{A_s} (Figure 21b). The fast advancement of the wetting front suggests that, in these cases, the peaks might have occurred between 0.5 and 5 days, hence they are not shown in Figure 21b. Conversely, the COV_{A_s} for $m = 0.2$ exhibits a sharp peak indicating a large spread of failure mechanisms at 5 days and hence a large variation of A_s between realisations as previously discussed. As before, the slower

advancement of the wetting front delays the attainment of the peak value of COV_{A_s} to 10 days for the two cases of $m = 0.4$ and 0.8 (Figure 21b).

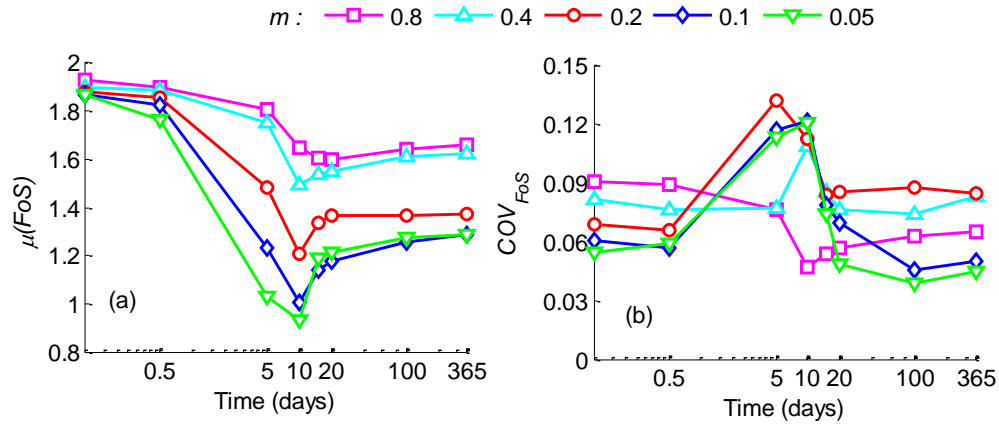


Figure 20: Time evolution of FoS in terms of mean (a) and coefficient of variation (b).
Analyses: influence of the SWRC (parameter m).

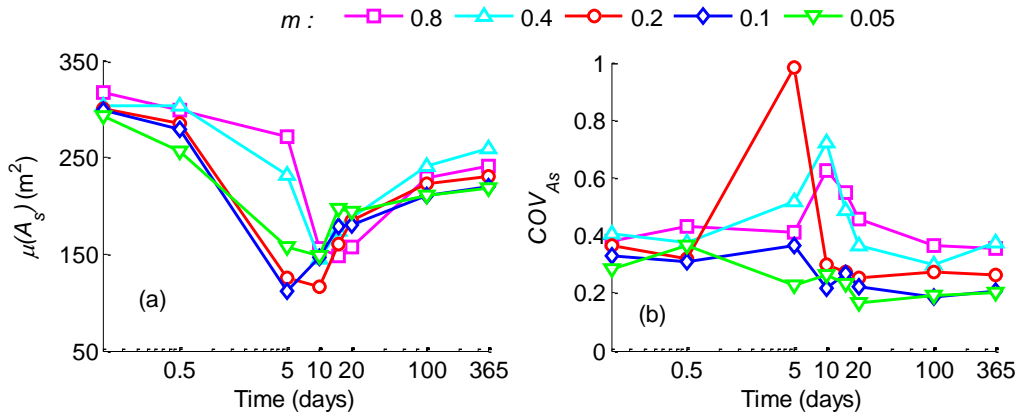


Figure 21: Time evolution of A_s in terms of mean (a) and coefficient of variation (b).
Analyses: influence of the SWRC (parameter m).

5 Conclusions

This study has shown that the interaction between randomly heterogeneous porosity and partial saturation can lead to very complex statistical variations of both factor of safety and failure size in soil slopes exposed to rainfall infiltration. In general, infiltration diminishes the stability of an unsaturated slope but the extent of this effect depends on various factors. If the slope exhibits large porosity variability, results can change significantly among realisations and fluctuate considerably over time, which may lead to different conclusions about the safety of the slope compared to the homogeneous case. Moreover, the statistical variation of the factor of safety and failure size is strongly influenced by other factors such as water table depth, rainfall intensity, saturated permeability and retention parameters.

The advancement of the wetting front during rainfall has a strong influence on both factor of safety and failure size. If the wetting front attains or surpasses a 'critical' depth, failure is confined within the wetted superficial layer with a relatively low factor of safety. Conversely, if the wetting front is shallower than the critical depth, the failure surface penetrates deep in the soil, through both wetted and unwetted regions, with a relatively high factor of safety. During rainfall, the mean values of both factor of safety and failure size decrease because of the progressive reduction of soil suction in the superficial soil layer. These mean values attain their respective minima when the majority of Monte Carlo realisations exhibit wetting fronts deeper than the critical depth. After the end of the rainfall, these mean values increase again as suction is progressively recovered. The coefficients of variation of both factor of safety and failure size also increase until the wetting front attains the critical depth in a significant number of realisations. At this time, the failure mechanism may vary widely from shallow to deep seated, which produces large coefficients of variation.

An increase in rainfall intensity leads to a faster drop in suction, which elevates the risk of failure. Conversely, a progressive increase of saturated permeability only elevates the risk of failure up to a limit, after which the probability of failure starts to reduce. This is

because a very high permeability allows excess pore water pressures to dissipate quickly while a very low permeability impedes infiltration altogether. Both these effects decrease the possibility of failure, which explains why the highest risk corresponds to an intermediate permeability level.

The effect of porosity on unsaturated permeability is non-monotonic due to the opposite variation of the saturated and relative permeability. This complex behaviour produces rather unexpected patterns of water flow in heterogeneous unsaturated slopes. If the retention curve is independent of porosity, water preferably migrates through high porosity regions but, if a pronounced dependency on porosity is introduced, water tends to move through low porosity areas. Moreover, the risk of failure is significantly higher if a dependency of water retention on porosity is assumed and if the gradient of the retention curve is small to intermediate.

The progressive infiltration of water reduces both factor of safety and sliding area. This does not mean that a large sliding cannot occur in correspondence of a low factor of safety but only means that a small failure might initially occur triggering a progressively larger mechanism. It also suggests that a more accurate assessment of risk should be based on the likelihood of both slope failure and large sliding area.

6 Acknowledgements

The authors would like to acknowledge the support by the centre for research-based innovation Klima2050 - Risk reduction through climate adaptation of buildings and infrastructure to the publication of this paper.

7 References

Alonso, E.E.: Risk analysis of slopes and its application to Canadian sensitive clays. *Géotechnique* **26**(3), 453-472 (1976)

- Alonso, E.E., Lloret, A.: Evolution in time of the reliability of slope in partially saturated soils. Paper presented at the Fourth International Conference on Application of Statistics and Probability in Soil and Structural Engineering Bologna, Italy,
- Arnold, P., Hicks, M.A.: Stochastic modelling of unsaturated slope stability. Paper presented at the Fifth International Conference on Unsaturated Soils, Barcelona, Spain,
- Babu, G.L.S., Mukesh, M.D.: Effect of soil variability on reliability of soil slopes. *Géotechnique* **54**(5), 335-337 (2004)
- Baecher, G.B., Christian, J.T.: Reliability and statistics in geotechnical engineering. Wiley, Chichester, United Kingdom (2003)
- Bear, J.: Dynamics of Fluids in Porous Media. Dover, (1972)
- Bishop, A.W., Alpan, I., Blight, G.E., Donald, I.B.: Factors controlling the strength of partly saturated cohesive soils. Paper presented at the Regional Conference on Shear Strength of Cohesive Soils, Boulder,
- Cameron, D.A., Jaksa, M.B., Wayne, P., O'Malley, A.: Influence of trees on expansive soils in southern Australia. In: Al-Rawas, A.A., Goosen, M.F.A. (eds.) Expansive soils: recent advances in characterization and treatment. p. 526. Taylor & Francis, London, UK (2006)
- Cho, S.E.: Probabilistic stability analyses of slopes using the ANN-based response surface. *Computers and Geotechnics* **36**, 787-797 (2009)
- Cho, S.E.: Probabilistic stability analysis of rainfall-induced landslides considering spatial variability of permeability. *Engineering Geology* **171**, 11-20 (2014). doi:<http://dx.doi.org/10.1016/j.enggeo.2013.12.015>
- Cho, S.E., Lee, S.R.: Instability of unsaturated soil slopes due to infiltration. *Computers and Geotechnics* **28**(3), 185-208 (2001)
- Dou, H.-q., Han, T.-c., Gong, X.-n., Zhang, J.: Probabilistic slope stability analysis considering the variability of hydraulic conductivity under rainfall infiltration–redistribution conditions. *Engineering Geology* **183**, 1-13 (2014). doi:<http://dx.doi.org/10.1016/j.enggeo.2014.09.005>
- El-Ramly, H., Morgenstern, N.R., Cruden, D.M.: Probabilistic assessment of stability of a cut slope in residual soil. *Géotechnique* **55**(1), 77-84 (2005)
- Escario, V., Saez, J.: The shear strength of partly saturated soils. *Géotechnique* **36**(3), 453-456 (1986)
- Fenton, G.A.: Simulation and analysis of random field. Ph.D, Princeton University (1990)
- Fenton, G.A., Griffiths, D.V.: A slope stability reliability model. In, London, Ontario 2005. Proceeding of the K.Y.Lo Symposium
- Fredlund, D.G., Morgenstern, N.R., Widger, R.A.: The shear strength of an unsaturated soil. *Canadian Geotechnical Journal* **15**(3), 313-321 (1978)
- Gan, J.K., Fredlund, D.G., Rahardjo, H.: Determination of the shear strength parameters of an unsaturated soil using the direct shear test. *Canadian Geotechnical Journal* **25**(3), 500-510 (1988)
- Griffiths, D.V., Fenton, G.A.: Probabilistic Slope Stability Analysis by Finite Elements. *Journal of Geotechnical and Geoenvironmental Engineering* **130**(5), 507-518 (2004)
- Griffiths, D.V., Huang, J., Fenton, G.A.: Probabilistic Slope Stability Analysis using RFEM with Non-Stationary Random Fields. In: Schweckendiek, T.T., Tol,

- A.F.F.v., Pereboom, D.D., Staveren, M.T.M.v., Cools, P.M.C.B.M.P. (eds.) *Geotechnical Safety and Risk V Rotterdam, Netherlands 2015*, pp. 704 - 709
- Griffiths, D.V., Marquez, R.M.: Three-dimensional slope stability analysis by elastoplastic finite elements. *Geotechnique* **57** (2007)
- Hicks, M.A.: Risk and variability in geotechnical engineering. *Géotechnique* **1**(55), 1-2 (2005)
- Hicks, M.A., Chen, J., Spencer, W.A.: Influence of spatial variability on 3D slope failures. In: Brebbia, C.A., Beriatos, E. (eds.) *Proceedings of 6th International Conference on Computer Simulation in Risk Analysis and Hazard Mitigation, Thessaly, Greece 2008*, pp. 335-342
- Hicks, M.A., Onisiphorou, C.: Stochastic evaluation of static liquefaction in a predominantly dilative sand fill. *Géotechnique* **55**(2), 123–133 (2005)
- Hicks, M.A., Samy, K.: Influence of heterogeneity on undrained clay slope stability. *Quarterly J. Engineering Geology and Hydrogeology* **35**(1), 41–49 (2002)
- Hicks, M.A., Spencer, W.A.: Influence of heterogeneity on the reliability and failure of a long 3D slope. *Comput Geotech* (2010). doi:doi:10.1016/j.compgeo.2010.08.001
- Kozeny, J.: Über kapillare Leitung des Wassers im Boden. *Akad. Wiss. Wien* **136**(2a), 271-306 (1927)
- Lacasse, S., Nadim, F.: Uncertainties in characterizing soil properties. In: C. D. Shackelford, Nelson, P.P. (eds.) *Uncertainty in the geologic environment*. pp. 49-75. ASCE, New York (1996)
- Le, T.M.H.: *Stochastic Modelling of Slopes and Foundations on Heterogeneous Unsaturated Soils*. The University of Glasgow (2011)
- Le, T.M.H., Eiksund, G., Strøm, P.J.: Statistical characterisation of soil porosity. In: Deodatis, G., Ellingwood, B., Frangopol, D. (eds.) *Proceeding of the 11th International Conference on Structural Safety & Reliability, Columbia University, New York, USA, June 16 - 20, 2013* 2013. CRC Press/Balkema
- Le, T.M.H., Gallipoli, D., Sánchez, M., Wheeler, S.: Stability and failure mass of unsaturated heterogeneous slopes. *Canadian Geotechnical Journal* **52**(11), 1747-1761 (2015). doi:10.1139/cgj-2014-0190
- Le, T.M.H., Gallipoli, D., Sanchez, M., Wheeler, S.J.: Stochastic analysis of unsaturated seepage through randomly heterogeneous earth embankments. *International Journal for Numerical and Analytical Methods in Geomechanics* **36**(8), 1056-1076 (2012). doi:10.1002/nag.1047
- Mostyn, G.R., Li, K.S.: Probabilistic slope analysis: state-of-play. In, Canberra, Australia 1993. *Proceedings of the conference on probabilistic methods in geotechnical engineering*, pp. 89-109
- Mostyn, G.R., Soo, S.: The effect of autocorrelation on the probability of failure of slopes. In: *Proceedings of 6th Australia, New Zealand Conference on Geomechanics: Geotechnical Risk 1992*, pp. 542-546
- Olivella, S., Gens, A., Carrera, J., Alonso, E.: Numerical formulation for a simulator (CODE-BRIGHT) for the coupled analysis of saline media. *Engineering Computations* **13**(7), 87-112 (1996)
- Pathak, D.R., Gharti, H.N., Singh, A.B., Hiratsuka, A.: Stochastic modeling of progressive failure in heterogeneous soil slope. *Geotech Geol Eng* (2007)

- Phoon, K.-K., Santoso, A., Quek, S.-T.: Probabilistic Analysis of Soil-Water Characteristic Curves. *Journal of Geotechnical and Geoenvironmental Engineering* **136**(3), 445-455 (2010). doi:doi:10.1061/(ASCE)GT.1943-5606.0000222
- Rodríguez, R., Sánchez, M., Lloret, A., Ledesma, A.: Experimental and numerical analysis of a mining waste desiccation. *Canadian Geotechnical Journal* **44**, 644-658 (2007)
- Santoso, A.M., Phoon, K.-K., Quek, S.-T.: Effects of soil spatial variability on rainfall-induced landslides. *Computers and Structures* **89**(11-12), 893-900 (2011). doi:10.1016/j.compstruc.2011.02.016
- Sejnoha, M., Sejnoha, J., Kalousková, M., Zeman, J.: Stochastic analysis of failure of earth structures. *Probabilistic Engineering Mechanics* **22**(2), 206-218 (2007)
- Tsaras, I., Rahardjo, H., Toll, D.G., Leong, E.C.: Controlling parameters for rainfall-induced landslides. *Computers and Geotechnics* **29**(1), 1-27 (2002)
- UPC: CODE_BRIGHT User's Guide: A 3-D program for thermo-hydro-mechanical analysis in geological media. Cent. Int. de Metodos Numericos en Ing. Univ. Politecnica de Catalunya, Department of Geotechnical Engineering and Geosciences, Barcelona, Spain (2010)
- van Genuchten, M.T.: A closed form equation for predicting the hydraulic conductivity of unsaturated soils. *Soil Science Society of America Journal* **44**, 892-898 (1980)
- van Genuchten, M.T., Nielsen, D.R.: On describing and predicting the hydraulic properties of unsaturated soils. *Annales Geophysicae* **3**(5), 615-627 (1985)
- Xia, Y., Mahmoodian, M., Li, C.-Q., Zhou, A.: Stochastic Method for Predicting Risk of Slope Failure Subjected to Unsaturated Infiltration Flow. *International Journal of Geomechanics* **17**(8) (2017)
- Zandarín, M.T., Oldecop, L.A., Rodríguez, R., Zabala, F.: The role of capillary water in the stability of tailing dams. *Engineering Geology* **105**, 108-118 (2009)
- Zhang, J., Huang, H.W., Zhang, L.M., Zhu, H.H., Shi, B.: Probabilistic prediction of rainfall-induced slope failure using a mechanics-based model. *Engineering Geology* **168**, 129-140 (2014). doi:<http://dx.doi.org/10.1016/j.enggeo.2013.11.005>
- Zhang, L.L., Zhang, L.M., Tang, W.H.: Technical note: Rainfall-induced slope failure considering variability of soil properties. *Géotechnique* **55**(2), 183-188 (2005)
- Zhu, T.: Some Useful Numbers on the Engineering Properties of Materials -GEOL 615 Course note
<http://www.stanford.edu/~tyzhu/Documents/Some%20Useful%20Numbers.pdf>
 (2014). Accessed 23 May 2014